How to Cite:
Ayyavaraiah, M., & Venkateswarlu, B. (2022). Ensemble classification based COVID-19 diagnosis from chest X-rays and CT images. *International Journal of Health Sciences*, *6*(S3), 1964–1983. https://doi.org/10.53730/ijhs.v6nS3.5905

Ensemble classification based COVID-19 diagnosis from chest X-rays and CT images

Monelli Ayyavaraiah
Research Scholar, Dayananda Sagar University-Bangalore, Assistant Professor, Department of Computer Science and Engineering, KKR & KSR Institute of Technology & Sciences (KITS), Vinjanampadu, Vatticherukuru Mandal, Guntur-522017
Email: ayyavaraiah50@gmail.com

Bondu Venkateswarlu
Associate Professor, Dayananda Sagar University-Bangalore.
Email: bonduvenkat-cse@dsu.edu.in

***Abstract*---**COVID-19 continues to have catastrophic impacts on human beings lives all over the world. To fight with this disease, it has been required to screen the impacted patients rapidly with less false alarming. Moreover, the significant feasible steps to attain this objective are computer-aided methods of machine learning strategies trained by the features of the CT and chest X-ray images. However, these features' high dimensionality becomes a critical issue that often reflects as high in false alarming in disease scope prediction. Concerning to the stated argument, this contribution endeavored to portray an ensemble learning-based machine learning approach to reduce the feature overfitting due to of high dimensionality in training-corpus for COVID-19 disease prediction with minimal false alarming. The proposed method's cross-validation using benchmark dataset evincing the minimal false alarming in COVID-19 disease prediction using high dimensional features of the radiographic test reports (x-ray and CT-images).

***Keywords*---**x-ray, CT-images, WHO, COVID-19, GLCM features, KS-Test.

Introduction

The "Severe Acute Respiratory Syndrome Coronavirus 2" in short referred as Covid-19 was first identified in first month of 2020 [1]. The initial cases were noticed at Wuhan, China [2]. The quick increase in mortality rate and illness

collapsed people's health all over the world at first, even though it was not deemed catastrophic. On January 30, 2020, the World Health Organization (WHO) labeled this endemic a public-health crisis of worldwide significance [3]. According to [4] the total number of coronavirus cases is 25, 297, 383 worldwide, with 6, 825, 774 active cases and 848,561 fatality cases as of 30 August 2020. Furthermore, every country, from industrialized to developing, has been combating this devastating epidemic, despite a lack of resources, inadequate diagnostic procedures, and poor healthcare infrastructure. Severe respiratory problems, fever, and cough are all indications of COVID-19 [5]. According to contribution [6], the most often utilized assays for COVID-19 identification are RT-PCR (reverse-transcription polymerase-chain-reaction). Furthermore, this test employs reverse transcription to extract DNA and then uses PCR to analyze DNA amplification. As this virus contains RNA, it might be used to detect COVID-19 [7].

Nonetheless, there are a number of limitations to this test. Furthermore, Covid-19 test delivers significant results if performed after few hours of the symptoms appeared. Nonetheless, this test-kit has not been widely distributed. The work [8] shows that it is unreliable since it may provide false-negative results, implying that it may falsely classify positive patients as healthy. As a result, clinicians and the healthcare system have had tremendous difficulties in combating the epidemic. Given the infectious nature of the virus, it has been swiftly spreading. Several nations have indicated that they would stay at home and have declared a state of emergency to slow the spread of the outbreak and prevent it, citing a scarcity of ICU admission, availability of ventilators as well as vaccines [9].

Nonetheless, quarantine and RT-PCR are insufficient for averting this pandemic, therefore researchers have been attempting to come up with alternative solutions. Furthermore, as described in [10], they concentrated on radiological image analysis for COVID-19 diagnosis. In this case, image analysis of chest radiography or CT scans may play a significant role. According to the researchers, COVID-19 is infected by CT scan pictures or X-rays with specific characteristics such as indistinct dark dots or ground glass opacity, which might aid in COVID-19 detection [11]. These images have been analyzed by radiologists and helps doctors in recognizing COVID-19 in the beginning stage. Nevertheless, in this pandemic, we require more quick, advanced, and available system. Manual image analysis might be time taking procedure; the parameter time has been more significant in this rapid spreading of COVID-19. More advanced, COVID-19 detection strategies have been developed and are required to diagnose with extreme pressure decrement on radiologists' services.

Deep learning model is widely playing key role in healthcare system, which has exhibited higher progression for automatic disease identification like identification of chest disease [12], detection of tumor [13], analysis of genomic sequence [14] and detection of cancer cell [15]. The work [16] projected a approach based on Deep-learning for identifying irregular density in the images of chest X-ray. Moreover, system utilized 3 CNN approaches for identifying abnormal or normal densities of images in chest x-ray. Besides, dataset comprises of 400 chest X-ray images, out of which test images are 100 and training images are 300. Moreover, these images labeled to be abnormal and normal as 1 and 0 in respective order.

Extensive simulations presented an accuracy of 96% for this model. Several researchers have been working currently for building automatic COVID-19 detection system based on DNN as in [17]. Also, they have proposed numerous DNN approaches for the extraction of feature from infected COVID-19 chest X-ray images, hence assuring optimal specificity, accuracy, and sensitivity. Many of them trained their approach on small dataset because of deficiency in image sources of COVID-19. Hence, these contributes require additional improvement by appropriate training as well as testing the model in practical.

Related work

From starting of this pandemic COVID-19, several researchers are endeavoring to deliver AI based prediction models for COVID-19 detection. In this segment, current studies associated to detection of COVID-19 based on ML or DNN ensemble classifiers have been explained. In table 1, comparative study of current research has been presented. The work [18] projected a novel deep CNN approach and DeTrac depending on images of chest C-ray. Also, system optimized the dataset local structure by implementing class-decomposition layer. Consequently, system training has been performed by utilizing pre-trained ResNet approach. Ultimately, class-composition-layer has been utilized for tuning final-classification. Moreover, dataset incorporated chest X-ray images are 105 for COVID-19, SARS virus disease images are 11, and normal chest X-ray images are 80. Extensive simulations attained a sensitivity of 97.91%, specificity is 91.87% and accuracy is 95.12% for this model. The work [19] projected generative adversarial system with DNN. Also, dataset comprised of chest X-ray images of COVID-19, pneumonia virus, and bacterial of count 69, 79, and 79 in respective order. Moreover, research has been carried out by utilizing pre-trained approaches. Amongst these approaches, Google net attained an accuracy of 80.6% for 4 classes' classification. Also, Alex-Net attained an accuracy of 85.2% in 3 cases of class, and finally Google net attained an accuracy of 100% in 2 class set-ups. The work [20] developed numerous DNN for COVID-19 automatic classification. The pre-trained approaches utilized for system are ResNet50V2 and Exception. This dataset comprised of 180 images of X-ray of COVID-19 patients, pneumonia affected patients' images are 6054 and normal patient's images are 8851. Extensive simulations exhibited average accuracy of 91.4% for overall classes.

The work [21] projected CNN based on patch with comparatively smaller amount of trainable aspects. Moreover, this system had chosen ultimate classification decision by highest voting from outcomes at several locations of path. Dataset comprised of images 15043 incorporating COVID-19 images are 180, pneumonia images are 6012 and normal patients are 8851. Also, extensive simulation exhibited F1-score are 84.4%, recall as 85.9%, precision as 83.4% and accuracy of 88.9%. The work [22] projected novel model based on deep learning based on X-ray images of chest. Also, this system has been comprised of 3 modules: network backbone for extracting features of X-ray images of chest at high-level, classification-head for producing the score of classification and head of anomaly detection for generating score of scalar anomalies. Furthermore, dataset comprised of covid-19 patient's chest x-ray images are 100, pneumonia instances are 1431 images. Extensive simulations presented specificity of 70.65%, and

sensitivity as 96% for this model. The work [23] proposed numerous pre-trained CNN model for detection of COVID-19. Moreover, transfer learning has been utilized by system for diagnosing with comparatively smaller dataset of COVID-19. The experimentation has been carried out with 2 datasets. Primary dataset comprised of X-ray images as 1427 by incorporating normal cases as 504, bacterial pneumonia images as 700 and COVID-10 affected cases as 224. Next dataset comprised of x-ray images of COVID-19 as 224, normal cases as 504 and viral and bacterial pneumonia images as 700. Amongst pre-trained approaches, MobileNetV2 attained sensitivity as 98.66%, specificity as 96.46% and accuracy as 96.78% for secondary dataset.

The work [24] projected a novel deep approach called CovXNet by utilizing X-ray images of chest to detect the automatically detection COVID-19 and other instances of pneumonia. Moreover, system projected convolution of depth-wise for extracting radiomic features from X-ray images of chest. Initially, they trained their model with chest X-ray of both infected and healthy classes. Furthermore, system utilized stacking algorithm and discriminative localization based on gradient. This dataset comprised of COVID-19 cases of 305 images, bacterial pneumonia images as 2780, normal patient's images are 1583 and viral pneumonia images are 1493. Extensive experimentations presented an accuracy of 97.4% for normal cases vs COVID-19 and also attained an accuracy of 90.2% for classification amongst bacterial pneumonia, viral and normal, COVID -19 cases. The work [25] proposed a model based on deep-learning for diagnosing COVID-19 from X-ray images of chest. The dataset comprised for COVID-19 are 122 images, 150 images of bacterial pneumonia, 150 images of normal case images and viral pneumonia images are 150. This system exhibited accuracy and specificity as 100% and sensitivity as 99% for 4 classes' classification. The work [26] projected a model, where 9 distinct pre-trained approaches extracted the features from the images of chest X-ray. Moreover, this system utilized SVM for categorizing COVID-19 by utilizing features extracted. Overall X-ray images of chest are 381 and have been utilized as dataset for simulation. Amongst overall approaches, ResNet 50 has been considered as optimal for extraction of feature. The work [27] proposed a strategy, where 4 divergent pre-trained approaches have been utilized. Also, dataset comprises of COVID-19 samples of 115, healthy samples are 60361 and pneumonia cases are 322. Amongst these approaches, VGG19 and VGG16 are optimal. The model VGG19 attained accuracy of 81% for pneumonia versus COVID-19 classification. The work [28] developed novel ensemble approach depending on ML classifiers for predicting the diabetic patients. This system projected 6 ML approaches such as NB, random-forest, decision trees, KNN, XG boost and AdaBoost. Weighted ensemble has been utilized by this system. These weights have been computed from ROC curve area of ML approaches. Furthermore, the system carried out this simulation with 500 and 268 non-diabetic and diabetic patients in respective order. Extensive simulation attained specificity as 93.4% ad sensitivity as 78.9% for the system.

The work [29] depicted 3-class design, which might distinguish among normal, COVID-19 and viral cases. The process based on segmentation attained an 86.7% of accuracy with CT scan sample images are 618. The work [30] stated swift AI development cycle with CT image analysis based on deep-learning. The works [31] [32] depicts open-source datasets incorporating X-ray images of COVID-19. The

researchers recommend a open source consolidated dataset besides with deep CNN approach called COVID-Net for novel coronavirus classification. The COVID-Net approach implements CNN framework with inputs as Chest X-ray images. Moreover, these approaches accomplish 93.3% of accuracy with definite images of COVID-19. The work [33] stated a model based on capsule called COVID-CAPS. Further, dataset comprises of general thorax diseases X-ray images are 94323. From the repository of NIH, the data has been extracted, which comprises of validation and training data with 0.9:0.1 split ratio. Also, this network attained sensitivity as 90%, specificity as 95.8% and 95.7% of accuracy.

The work [34] presents fine-tune, which is a retrained approach squeeze Net by utilizing Bayesian optimization process for categorizing related infections of coronavirus in images of X-ray. This dataset contains COVID-19 images as 66, normal chest images are 1349 and pneumonia are 3895 in a 0.8:0.1:0.1 split ratio. The work [35] implement Exception retrained deep approach for classifying COVID-19 images automatically in the images of chest X-rays. Also, dataset contains viral as 327, normal images are 310, coronaviruses are 284 and bacterial pneumonias as 330. Moreover, design attained 87.5% of accuracy, 95% of 4-class problem & 3-class problem on smaller dataset. ML based Covid-19 prediction using x-rays [36] [37] were using radiomic features to classify the state of COVID-19 test. The texture as well as morphological characteristics [36] and synthetic features hypothesized from overall radiomic features [37] were examined. Ensemble of multiple classifiers were used in [36] to reduce the impact of high dimensionality caused by over fitted data of the features. The method in [37] has hypothesized the synthetic features to reduce the dimensionality of the features. However, these methods succeeded to reduce the dimensionality by limiting or pruning the features in use, which often causes sever false alarming in prediction analytics.

Materials and Methods

Training the classifiers with appropriate features is essential for improving the quality. Thus, for the chosen model, the classifiers are trained using the x-ray/CT images. The images are used for extraction of morphological features, entropies, fractal dimensions, GLSM, and texture. The features extracted were optimized to train the supervised learning-based classifiers. Among the mentioned features, two critical features used for training are morphological and textual features. The pre-processing stages are used for conversion of the images to grayscale images and thus eliminating any kind of noises implicit to the images. In further process, the feature extraction is carried out from the gray-scale images. Significant diversity is observed in the chest x-ray images of the Covid-19 suspected cases. In the proposed model, fifty one features were chosen for analysis, wherein the table below refers to the set of features quantity in each of the segment.

Feature	Qty.
Fractal Dimensions	01
LBP	06

Entropy	05
GLCM	19
Morphological	09

Entropy

Entropy refers to the action of assessing the randomness that can be resourceful for texture characterizing the image input. The value of such randomness assessment is resourceful in the instances of matrix elements being identical. Using the entropy process, the segregation of the normal and the affected depiction of x-ray images are carried out. In the entropy process, uncertainty levels are high, and it is evident in the form of negative and positive chest x-ray images. [38]. Five kind of entropies are available for handling the process. Using the entropy process, in the proposed model, the classification of the scanned images of covid-19 prone and unaffected images are classified and segregated.

GLCM features

GLCM matrix is resourceful in classification of the distinction in the gray-shades of image. The computations in terms of texture features are assessed using the GLCM for assessing the conditions of pixel intensity changes. In general, over a matrix co-occurrence, it is assessed on the basis of the relative-distance d over the paid of pixels, which are assessed based on the number of pixels, and the respective structure. Despite the scope of numerous probabilities of mixture composition, in general it is quantized in 4 segments. Various set of GLCM features were discussed in [39] and [40], which are vital in structuring the texture [40].

Grey Level Run Length Matrix (GLRLM)

GLRLM is adapted for analyzing the gray-scale image related granular structures. GLRLM technically indicates the quantum of pixel runs in a run length j, corresponding to gray-level I in a specific direction. For each of the image fragment samples, the GLRLM is developed, and the gray-level run is indicative based on the consecutive set of pixels having the identical gray levels. Length of a run is defined by the cumulative number of pixels, and the features refers to the gray-scale image centric granular structure. RLM which is a two dimensional vector refers to the direction of the gray value i for the gray-scale image I (x,y), wherein it is utilized for focusing on the categorical aspects of features of distinct textures, resulting in terms of GLNU, SRE, and LRE [40].

Fractal dimensions

Fractal dimensions is used for detection of the surface coarseness over the gray-scale image and is depicted for further analysis [41]. 2D image processing model is adapted to identify the surface coarseness from the infected chest x-ray images. The corresponding difference between the images carrying the affected and unaffected are easy to trace based on the fractal dimensions. The divergences are traced using a sequential algorithm approach [42], and the variance box-counting is developed.

Local Binary-Patterns

LBP is the distinct set of feature extraction model, wherein the two critical factors like the neighborhood and the bilinear interpolation are used. The model is adapted as substantial support assessing any contrasts in the image, and profoundly used for assessing statistical and structural texture examination. LBP provides information in terms of minor primitives referred as Textron's. Certain associated features for the same of Volume-LBP and LPQ (Local Phase Quantization). LBP attributes are discussed more [43] and the application of LBP in the proposed model is more about focusing on the bilinear interpolation, and circular neighborhood, which is resourceful for LBP computation.

Let P_{ix} be pixels set observed for the range R chosen on the given chest x-ray image I. The pixel evident at the center of the range R indicates as p_c,
Let the vector Gp_c portrays the grey-scale values of the pixels, wherein neighboring pixels of the center p_c are represented.
In furtherance every pixel $\{p \exists p \in P_{ix} \wedge p \neq p_c\}$ is transformed into binary/Boolean patterns in order that the pixel exists in the vector Gp_c by the value 1, and the rest refers by 0.

The morphologic features

The morphometric features [44] and invariant moments [45] are technically perceived as resourceful morphological features. Such morphological features are critical in terms of observing any kind of similarities or divergence over the images used for training and to be tested for labeling.

Diversity assessment measures

This section explores the different distribution diversity assessment methods fusing to perform optimal feature selection fusion. The methods Wilcoxon signed-rank [46], Kolmogorov–Smirnov test [47], Mann Whitney U test [48], and Dual tailed t-Test [49] have used to perform a fusion of diversity estimation measures for optimal features selection.

Goodness-of-Fit-Test

The KS-test statistics indicate the distance amid accumulative distribution and experimental sample distribution, or it might be reported as a difference amid two experimental distribution samples of equal or diversified sizes. The goodness of fit state for the provided two datasets has been depicted through a distance metric that is called as Kolmogorov-Smirnov test [47]. Further, this metric does not require any information related to data distribution type, which is mandatory for other distance metrics to estimate the distribution diversity. Also, the application process of the KS-test algorithmic approach has been explained below:

$ks\_test(v_1, v_2)$ Begin //The input arguments v_a, v_b are two vectors.

Primarily, the process predicts the aggregation $Ag(v_a), Ag(v_b)$ of vectors v_a, v_b in respective order. Further, detects cumulative ratios are depicted in specified vectors v_a, v_b as corresponding sets CR_{v_a}, CR_{v_b} .

$$pr = 0$$

$$\underset{i=1}{\overset{|v_j|}{\forall}} \left\{ CR_{v_j} \leftarrow \left(pr += e_i * \left(Ag(v_j) \right)^{-1} \right) \exists e_i \in v_j \right\}$$

// Finding the cumulative ratio for each vector's entry v_a, v_b has been predicted.

Here in the above equation,
The representation e_i indicates every element of a vector v_j , the representation pr indicates the accumulative ratio of the previous element in reiteration, representation $Ag(v_j)$ indicates an aggregate of values represented in the v_j , and the set CR_{v_j} incorporates cumulative ratios of overall elements existed in v_j
Later identify the absolute cumulative ratios distance resulting in values, which are existed at an identical index of vectors v_a, v_b as stated below:

$$\underset{i=1}{\overset{\max(|CR_{v_a}|,|CR_{v_b}|)}{\forall}} \left\{ \begin{matrix} c_i(v_a), c_i(v_b) \exists \\ c_i(v_a) \in CR_{v_a} \wedge c_i(v_b) \in CR_{v_b} \end{matrix} \right\}$$

// for each i index, values existed in CR_{v_a}, CR_{v_b}

Begin

$$AD_{CR_{v_a} \leftrightarrow CR_{v_b}} \leftarrow abs\left(c_i(v_a) - c_i(v_b) \right)$$

// represents the absolute distance of cumulative ratios AD presents in sets" CR_{v_a}, CR_{v_b} at the index and preserves in a set $AD_{CR_{v_a} \leftrightarrow CR_{v_b}}$.

End

Identify d-stat, which would be the highest value that is existed in $AD_{CR_{v_a} \leftrightarrow CR_{v_b}}$

The d-critic aimed at KS-table has been identified for $Ag(v_a), Ag(v_b)$ provided for the degree of threshold probability $p\tau$

if d-stat that depicted is greater than d-critic presented, return 0 //2 vectors are not distinct.

Else return 1 //two vectors are distinct

End

Mann Whitney U Test

The well-recognized non-parametric test for comparing the results among two independent sets is the Mann-Whitney-U test (MWUT). Sometimes, this MWUT is also known as the Wilcoxon Rank Sum test, which has been utilized for testing whether two samples have been derived from a similar population. Some of the examiners understand this test by comparing medians among two populations. Also, recall, which is a parametric test used for comparing the means among independent sets.

The two-way and null study hypothesis focused towards non-parametric tests, on the other hand, one-way test reports as "If given samples of two distributions are not showing diversity, then return zero, else returns one." This test is frequently conducted as a two-way diversity assessment test, and so the study hypothesis denotes that samples have been different in the provided directionality. When attention is based on a positively or negatively shift in one sample against to others, the one-way study hypothesis is used. In addition, the test technique comprises combining data from two samples into a single integrated sample while taking note of source sample of each observation. Then, orders them from minimal to maximum and ranks them in the same order that begins at 1.

$mwu\_test(v_1, v_2)$ **//** Begin

the given vectors v_1, v_2 shall be sorted in ascending order

$$U(v_1) = 0$$

$$U(v_2) = 0$$

$\underset{i=1}{\overset{|v_1|}{\forall}} \{e_i \exists e_i \in v_1\}$ Begin //each element e_i

$\underset{j=1}{\overset{|v_2|}{\forall}} \{e_j \exists e_j \in v_2\}$ Begin //For each element e_j

$$U(v_1) += \begin{Bmatrix} 1 \exists (v_j < v_i) \\ 0 \end{Bmatrix}$$

$$U(v_2) += \begin{Bmatrix} 1 \exists (v_i < v_j) \\ 0 \end{Bmatrix}$$

End

End

$if\ (U(v_i) \neq U(v_j)$

$$U = \begin{Bmatrix} U(v_i) \exists (U(v_i) < U(v_j)) \\ U(v_j) \end{Bmatrix}$$

Determine the d-critic at distance threshold $d\tau(0.1, 0.05, or\ 0.01)$ from U-Table

$$return\begin{cases}1\exists(U > dc)\\0\end{cases}$$

End

Tailed-Test

The projected distribution diversity values for the features under 2 labels, where standard t-test ANOVA has been utilized. Also, the vector v_1 depicts projected values for features in records that are infected, and the vector v_2 indicates expected values for an identical feature in records. Further, two distribution diversity vectors v_1, v_2 have been measured by utilizing a t-test, and the procedure is in the following way, as shown in the below equation. The expected distribution diversity values for the features under two labels, calculated using a conventional tailed-test. The input vectors v_1, v_2 shows the values anticipated for a feature in the records labeled positive, and the values anticipated for the corresponding feature in negative records in the respective order. Later, diversity of the given two vectors were assessed using a tailed-test as given in the following expression.

$t-test(v_1, v_2)$ // Begin

$$t-score = \left(\langle v_1\rangle - \langle v_2\rangle\right) * \left(\sqrt{\sigma(v_1)+\sigma(v_2)}\right)^{-1}$$

The representations $\langle v_1\rangle, \langle v_2\rangle$ denotes the mean values of the respective distribution vectors. And the representations $\sigma(v_1), \sigma(v_2)$ denotes the deviations of the respective distribution vectors

Further determines the degree of probability (p-value) pv [50].

$$return\begin{cases}1\exists(pv < p\tau)\\0\end{cases}$$

//returns one to represent that the distribution vectors are diversified else returns zero

End

Dimensionality reduction

The FC-Means (Fuzzy C-Means) [51], [52] were utilized to decrease the overfitting values of the features of both classes positive and negative. The FC-Means method divides the input data into tuples, with each tuple containing a collection of records with a substantial correlation. The FC-Means allows each record to be the entry of multiple resulting clusters. Furthermore, this method assigns fitness to each data-point of each cluster, based on the distance between that data-point and the centroid. The closer the data-point is to the cluster's centroid, the closer their membership is to the corresponding cluster. After that, the cluster's centroid have been updated using the following equation

$$\mu_{ij} = \left[\sum_{k=1}^{c} \left(d_{ij} / d_{ik} \right)^{(2/m-1)} \right]^{-1} \quad \textbf{...(Eq 1)}$$

$$\forall_{j=1}^{|cods|} \left\{ v_j = \left(\sum_{i=1}^{n} \left(\mu_{ij} \right)^m x_i \right) * \left(\sum_{i=1}^{n} \left(\mu_{ij} \right)^m \right)^{-1} \right\} \quad \textbf{...(Eq 2)}$$

The Eq 1, Eq 2 notation n indicates the number of data points. The notation v_j depicts cluster's j^{th} centroids, whereas Index fuzziness is denoted by $m \in [1, \infty]$. The representation $cods$ indicates the set of all centroids of respective clusters. The representation μ_{ij} denotes fitness of the i^{th} data-point towards j^{th} cluster. The distance between j^{th} cluster centroid and i^{th} data-point denotes by notation d_{ij}. The noticeable intent of this fuzzy c-means is:

$$J(U,V) = \sum_{i=1}^{n} \sum_{j=1}^{c} \left(\mu_{ij} \right)^m \left\| x_i - v_j \right\|^2 \quad \textbf{...(Eq 3)}$$

$\left\| x_i - v_j \right\|$ // Eq 3 represents Euclidean distance among j^{th} cluster's centroid and i^{th} data-point

The classifier

The random-forest [53] algorithm falls under the category of supervised-learning algorithm that is usually trained by bagging approach. Furthermore, sign behind bagging approach is that learning approaches integration increases the results. From the name itself, it signifies that random-forest (RF) contains large amount of decision trees that perform as ensemble-classifier. Moreover, in RF, each individual-tree partition class estimation and most of the votes becomes as our estimation approach. The RF classifier is a correct choice for learning from several approaches, which are covariant relatively. This approach can determine as manifold decision trees designed from covariant relatively approaches by utilizing picked roots randomly. Other significant strength of RF is that every tree would not be impacted by other trees classification errors. Also, the mandate parameters required for enhancing the optimality of RF classification procedure are presented in below description. Some signals must be there in the features so that approaches designed by using those features have been optimal regardless of randomly guessing. Individual trees are having estimations and needed to have minimal correlations over one other. The RF explanation for the classification as follows: The RF algorithm for both classification and regression as follows:

- Draw samples of bootstrap n_{tree} from the original-data.
- For each samples of bootstrap, enhance an unpruned classification or regression tree with below variations: at each node, in spite of choosing the

optimum split amongst overall predictors, these sample random predictors m_{try} and choose the optimum split from amongst those variables.

- The new data has to be estimated by accumulating the estimations or predictions of n_{tree} trees. Moreover, prediction of error rate has been obtained based on data trained in the following way:
  - At bootstrap iteration, predict the information in sample of bootstrap by using grown tree in sample.
  - The estimations of OOB have to be accumulated. Measure the error rate and call it as error rate of OOB prediction.

The Pseudo model of the Random-Forest

Begin

Input:

N //The representation signifies the amount of nodes

M //The representation denotes the count of features

The representation D signifies count of trees.

The representation Output V signifies the class with highest votes

While //recurrent if the criteria is true **do**

Sample A bootstrap must be randomly drawn from data training, which has been depicted with D.

Following steps must be utilized for T_i tree constructing from sample A, which has been drawn as mentioned above A:

(1) Elect m features from M , while $m \ll M$

(2) Measure the optimum split-point amongst m features for d node

(3) Node is divided into 2 daughter nodes by using optimum split procedure.

(4) The phases 1, 2 & 3 are repeated until desired number of nodes is obtained.

Forest must be built by repeating from steps 1-4 that are recurrent for D iteration.

End

Set of resultant trees $\{T_i$

The new sample must be implemented for every built trees begins at root.

Sample must be assigned to class corresponding to the leaf-node.

Relate total decisions or trees votes.

V has been considered as output that is maximal class vote.

End RF Algorithm

Experimental study

In this empirical study, the overall amount of labeled records used is 816. It comprises positive labeled records as 46103 and negative labeled records are 35511. The work [54] used k-fold LPOCV (Leave-pair-out-cross validation) for measuring the projected models performance. Also, metrics of cross-validation have considered for measuring the projected model EC-C19D (ensemble classification-based COVID-19-Diagnosis). In respect to this, accuracy prediction, false alarm scope, label prediction robustness has been measured. The projected model has been compared with contemporary models like COVID-Classifier [37] and "Machine-learning classification of texture features of portable chest X-ray" (MLC-TF) [36].

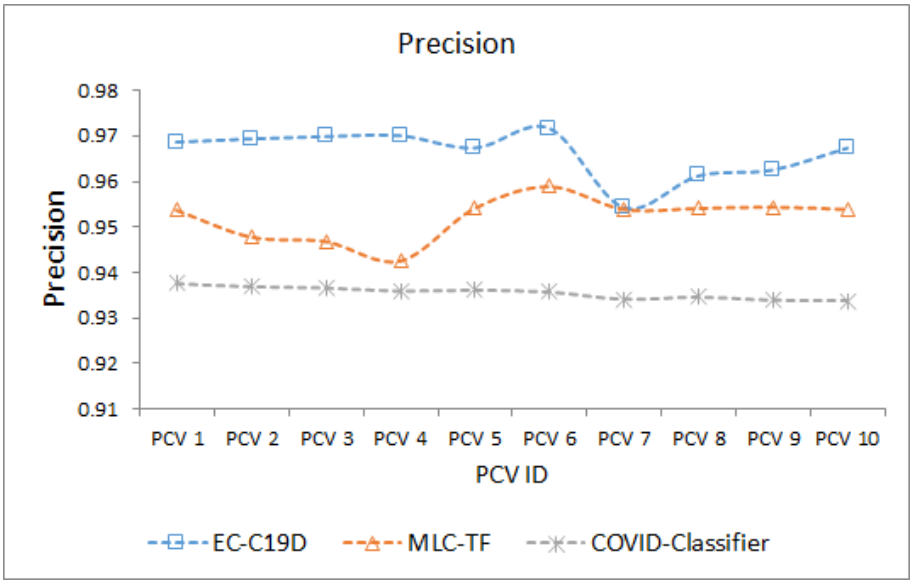

Figure 1. Precision of 10-folds of leave-pair-out cross-validation of EC-C19D, MLC-TF, and COVID-Classifier

Figure 1 shows a graph of precision metric and 10-folds of leave-pair-out cross-validation for the anticipated model EC-C19D as well as the existing models MLC-TF, and COVID-Classifier. Comparison has been made between projected models and contemporary models. From the above figure, it has been exhibited that, the model EC-C19D performance in terms of precision is more when compared to contemporary models MLC-TF, and COVID-Classifier. The model EC-C19D has been ranked last in precision because of dimensionality curse in training-corpus.

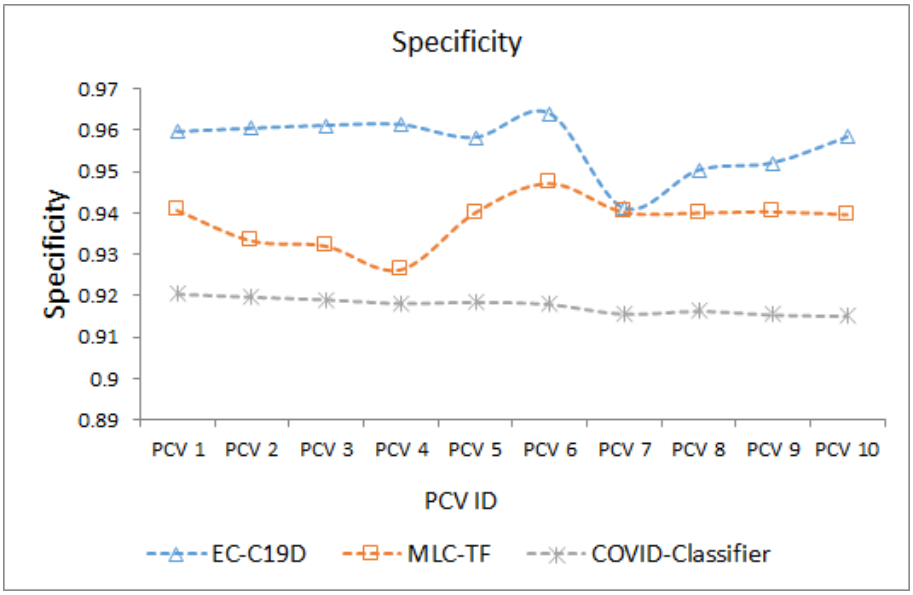

Figure 2. Specificity exhibited by 10-folds of leave-pair-out cross-validation of EC-C19D, MLC-TF, and COVID-Classifier

The metric specificity has been considered for measuring the performance of projected model EC-C19D and contemporary models MLC-TF, and COVID-Classifier. Graph has been presented among metric specificity and 10-folds of leave-pair-out cross-validation over these projected and contemporary models as shown in figure 2. Comparison has been made between projected models and contemporary models. From the above figure, it has been exhibited that, the model EC-C19D performance in terms of specificity is more when compared to contemporary models MLC-TF, and COVID-Classifier.

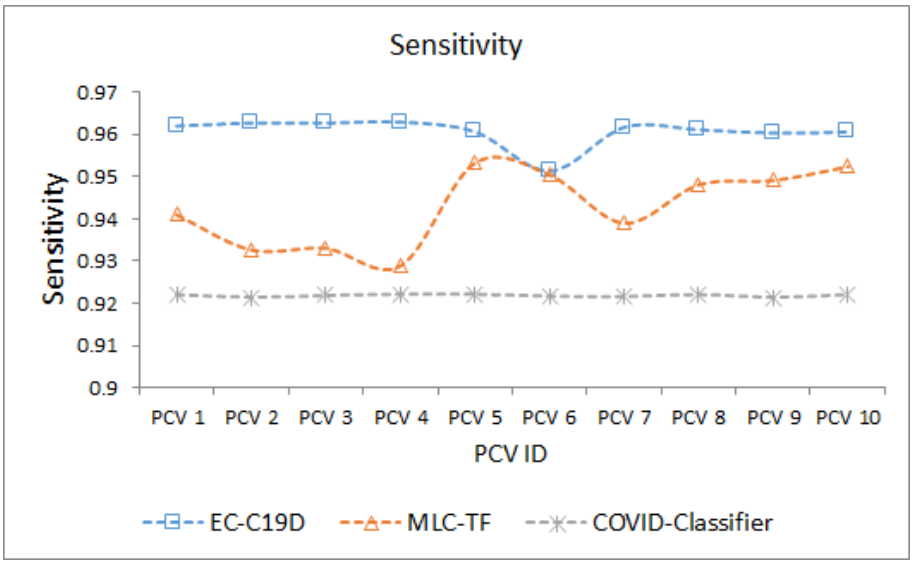

Figure 3. Sensitivity of 10-folds of leave-pair-out cross-validation of EC-C19D, MLC-TF, and COVID-Classifier

In figure 3, graph has been portrayed among Sensitivity metric and 10-folds of leave-pair-out cross-validation over the projected model EC-C19D and contemporary models MLC-TF, and COVID-Classifier. Comparison has been made between projected models and contemporary models. From the above figure, it has been exhibited that, the model EC-C19D performance in terms of Sensitivity is outperforming when compared to contemporary models MLC-TF, and COVID-Classifier. The model EC-C19D has been ranked last in Sensitivity because of dimensionality curse in training-corpus.

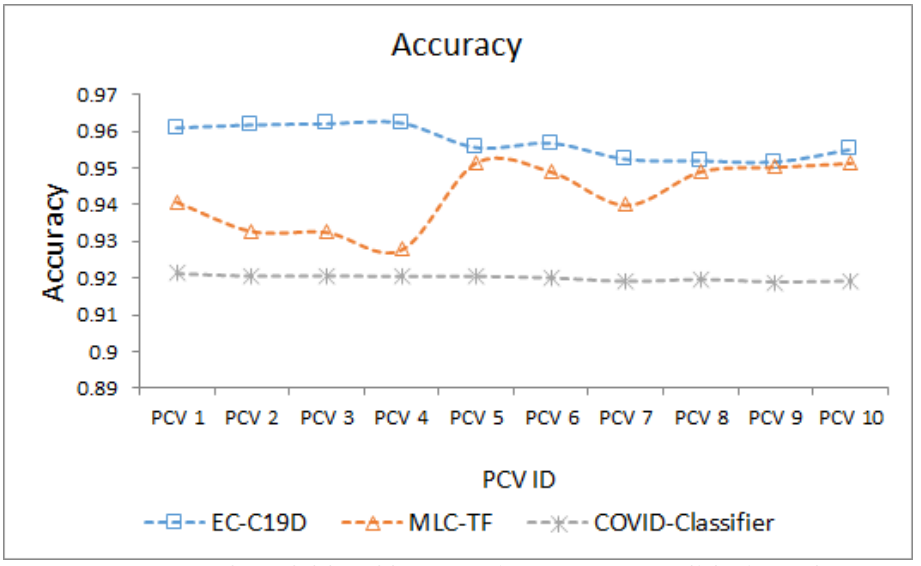

Figure 4. Accuracy of 10-folds of leave-pair-out cross-validation of EC-C19D, MLC-TF, and COVID-Classifier

The metric Accuracy has been considered for measuring the performance of projected model EC-C19D and contemporary models MLC-TF, and COVID-Classifier. Graph presents metric accuracy of 10-folds of leave-pair-out cross-validation over these projected and contemporary models as shown in figure 4. Comparison has been made between projected models and contemporary models. From the above figure, it has been exhibited that, the model EC-C19D performance in terms of accuracy is better when compared to contemporary models MLC-TF, and COVID-Classifier.

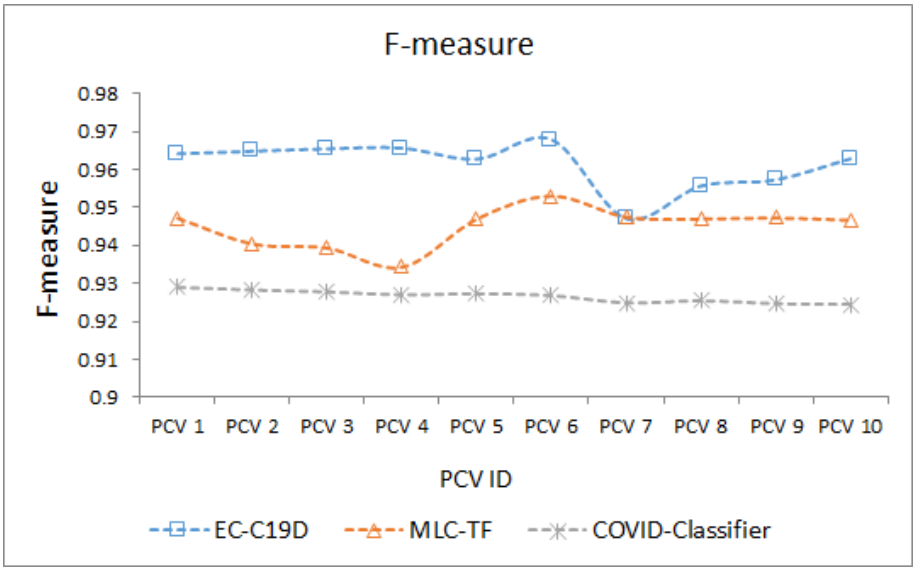

Figure 5. F-measure of 10-folds of leave-pair-out cross-validation of EC-C19D, MLC-TF, and COVID-Classifier

In figure 5, graph presents F-measure of 10-folds of leave-pair-out cross-validation over the projected model EC-C19D and contemporary models MLC-TF, and COVID-Classifier. Comparison has been made between projected models and contemporary models. From the above figure, it has been exhibited that, the model EC-C19D performance in terms of F1score is outperforming when compared to contemporary models MLC-TF, and COVID-Classifier.

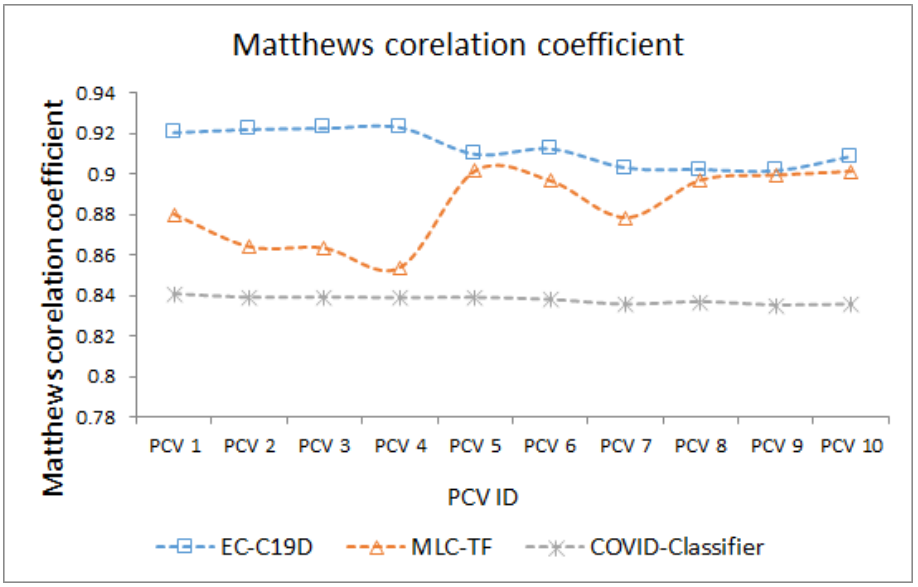

Figure 6. MCC of 10-folds of leave-pair-out cross-validation of EC-C19D, MLC-TF, and COVID-Classifier

The metric MCC has been considered for measuring the performance of projected model EC-C19D and contemporary models MLC-TF, and COVID-Classifier. Graph portrays metric MCC of 10-folds of leave-pair-out cross-validation over these projected and contemporary models as shown in figure 4. Comparison has been made between projected models and contemporary models. From the above figure, it has been exhibited that, the model EC-C19D performance in terms of MCC is better when compared to contemporary models MLC-TF, and COVID-Classifier.

Conclusion

Covid-19 pandemic impact has rippled the global healthcare conditions, and among the quickest measures essential for the prevention of spread and quality care is the early and accurate detection of the virus load, over a human being. The critical challenge facing the diagnostic centers are the overloaded samples for assessment, and the issues of accuracy emerging from sense of urgency and human errors. Thus, the AI based ensemble classification model discussed in this manuscript is aimed to reduce the inaccuracy issues and improve the overall speed of detection. The model is fundamentally about using the X-ray and CT-Scan images, wherein certain features are extracted, and an effective approach is designed that can help in quick and accurate labelling of the records as covid-19 positive or negative. The experimental study of the model using the appropriate

datasets indicate that the model is significant in comparison to the other two models chosen for detailed analysis.

References

1. Guan W, et al. Clinical characteristics of coronavirus disease 2019 in China. N Engl J Med 2020;382(18):1708–20. https://doi.org/10.1056/NEJMoa2002032.
2. Sun P, Lu X, Xu C, Sun W, Pan B. Understanding of COVID-19 based on current evidence. J Med Virol 2020;92(6):548–51. https://doi.org/10.1002/jmv.25722.
3. Bhagavathula AS, Aldhaleei WA, Rahmani J, Mahabadi MA, Bandari DK. Knowledge and perceptions of COVID-19 among Health care workers: crosssectional study. JMIR Public Heal. Surveill. 2020;6(2):e19160. https://doi.org/ 10.2196/19160.
4. Worldometer. Coronavirus update (live): cases and deaths from COVID-19 virus pandemic. Worldometers; 2020. https://www.worldometers.info/coronavirus/% 0Ahttps://www.worldometers.info/coronavirus/?. [Accessed Aug. 30 2020].
5. Zu ZY, et al. Coronavirus disease 2019 (COVID-19): a perspective from China. Radiology 2020;296(2):E15–25. https://doi.org/10.1148/radiol.2020200490.
6. Tahamtan A, Ardebili A. Real-time RT-PCR in COVID-19 detection: issues affecting the results. Expert Rev Mol Diagn 2020;20(5):453–4. https://doi.org/10.1080/ 14737159.2020.1757437.
7. Corman VM, et al. Detection of 2019 novel coronavirus (2019-nCoV) by real-time RT-PCR. Euro Surveill 2020;25(3). https://doi.org/10.2807/1560-7917.ES.2020.25.3.2000045.
8. Lauer SA, et al. The incubation period of coronavirus disease 2019 (CoVID-19) from publicly reported confirmed cases: estimation and application. Ann Intern Med 2020;172(9):577–82. https://doi.org/10.7326/M20-0504.
9. Corum J, Zimmer C. Coronavirus vaccine tracker - the New York Times. The New York Times; 2020. accessed Aug. 30, 2020, https://www.nytimes.com/interactiv e/2020/science/coronavirus-vaccine-tracker.html.
10. Islam MM, Karray F, Alhajj R, Zeng J. A review on deep learning techniques for the diagnosis of novel coronavirus (COVID-19). 2020 [Online]. Available: htt ps://arxiv.org/abs/2008.04815; 2020.
11. Xia W, Shao J, Guo Y, Peng X, Li Z, Hu D. Clinical and CT features in pediatric patients with COVID-19 infection: different points from adults. Pediatr Pulmonol 2020;55(5):1169–74. https://doi.org/10.1002/ppul.24718.
12. Hwang EJ, et al. Development and validation of a deep learning-based automated detection algorithm for major thoracic diseases on chest radiographs. JAMA Netw. open 2019;2(3):e191095. https://doi.org/10.1001/jamanetworkopen.2019.1095.
13. Mohsen H, El-Dahshan E-SA, El-Horbaty E-SM, Salem A-BM. Classification using deep learning neural networks for brain tumors. Futur. Comput. Informatics J. 2018;3(1):68–71. https://doi.org/10.1016/j.fcij.2017.12.001.
14. Quang D, Xie X. DanQ: a hybrid convolutional and recurrent deep neural network for quantifying the function of DNA sequences. Nucleic Acids Res 2016;44(11). https://doi.org/10.1093/nar/gkw226.

15. Cires¸an DC, Giusti A, Gambardella LM, Schmidhuber J. Mitosis detection in breast cancer histology images with deep neural networks. Lect Notes Comput Sci 2013; 8150 LNCS(PART 2):411–8. https://doi.org/10.1007/978-3-642-40763-5_51.
16. Kieu PN, Tran HS, Le TH, Le T, Nguyen TT. Applying Multi-CNNs model for detecting abnormal problem on chest x-ray images. In: Proceedings of 2018 10th international conference on knowledge and systems engineering, KSE 2018; 2018. p. 300–5. https://doi.org/10.1109/KSE.2018.8573404.
17. Islam MZ, Islam MM, Asraf A. A combined deep CNN-lstm network for the detection of novel coronavirus (COVID-19) using X-ray images. Informatics in Medicine Unlocked Aug. 2020;20:100412.
18. Abbas A, Abdelsamea MM, Gaber MM. Classification of COVID-19 in chest X-ray images using DeTraC deep convolutional neural network. Appl Intell 2020. https:// doi.org/10.1007/s10489-020-01829-7.
19. Loey M, Smarandache F, Khalifa NEM. Within the lack of chest COVID-19 X-ray dataset: a novel detection model based on GAN and deep transfer learning. Symmetry 2020;12(4). https://doi.org/10.3390/SYM12040651.
20. Rahimzadeh M, Attar A. A modified deep convolutional neural network for detecting COVID-19 and pneumonia from chest X-ray images based on the concatenation of Xception and ResNet50V2. Informatics Med. Unlocked 2020;19. https://doi.org/10.1016/j.imu.2020.100360.
21. Oh Y, Park S, Ye JC. Deep learning COVID-19 features on CXR using limited training data sets. IEEE Trans Med Imag 2020;39(8):2688–700. https://doi.org/ 10.1109/TMI.2020.2993291.
22. Zhang J, Xie Y, Li Y, Shen C, Xia Y. COVID-19 screening on chest X-ray images using deep learning based anomaly detection. 2020. aeXiv.2002.12338 vol. 1.
23. Apostolopoulos ID, Mpesiana TA. Covid-19: automatic detection from X-ray images utilizing transfer learning with convolutional neural networks. Phys. Eng. Sci. Med. 2020;43(2):635–40. https://doi.org/10.1007/s13246-020-00865-4.
24. Mahmud T, Rahman MA, Fattah SA. CovXNet: a multi-dilation convolutional neural network for automatic COVID-19 and other pneumonia detection from chest X-ray images with transferable multi-receptive feature optimization. Comput Biol Med 2020;122. https://doi.org/10.1016/j.compbiomed.2020.103869.
25. Tsiknakis N, et al. Interpretable artificial intelligence framework for COVID-19 screening on chest X-rays. Exp. Ther. Med. 2020. https://doi.org/10.3892/ etm.2020.8797.
26. Sethy PK, Behera SK, Ratha PK, Biswas P. Detection of coronavirus disease (COVID- 19) based on deep features and support vector machine. Int. J. Math. Eng. Manag. Sci. 2020;5(4):643–51. https://doi.org/10.33889/IJMEMS.2020.5.4.052.
27. Horry M, et al. X-ray image based COVID-19 detection using pre-trained deep learning models. 2020. https://doi.org/10.31224/osf.io/wx89s.
28. Hasan MK, Alam MA, Das D, Hossain E, Hasan M. Diabetes prediction using ensembling of different machine learning classifiers. IEEE Access 2020;8: 76516–31. https://doi.org/10.1109/ACCESS.2020.2989857.

29. X. Xu, X. Jiang, C. Ma et al., “A deep learning system to screen novel coronavirus disease 2019 pneumonia,” Engineering, vol. 6, no. 10, pp. 1122–1129, 2020.
30. O. Gozes, M. Frid-Adar, H. Greenspan et al., “Rapid AI development cycle for the coronavirus (COVID-19) pandemic: initial results for automated detection & patient monitoring using deep learning CT image analysis,” 2020, https://arxiv.org/abs/2003050372020.
31. L. Wang, Z. Q. Lin, and A. Wong, “COVID-net: a tailored deep convolutional neural network design for detection of COVID-19 cases from chest X-ray images,” Scientific Reports, vol. 10, no. 1, pp. 1–12, 2020.
32. J. Paul Cohen, P. Morrison, L. Dao, K. Roth Vector, T. Q. Duong, and M. Ghassemi Vector, “COVID-19 image data collection: prospective predictions are the future,” 2020, https://arxiv.org/abs/2006.11988.
33. P. Afshar, S. Heidarian, F. Naderkhani, A. Oikonomou, K. N. Plataniotis, and A. Mohammadi, “COVID-CAPS: a capsule network-based framework for identification of COVID-19 cases from X-ray images,” Pattern Recognition Letters, vol. 138, pp. 638–643, 2020.
34. F. Ucar and D. Korkmaz, “COVIDiagnosis-Net: Deep BayesSqueezeNet based diagnosis of the coronavirus disease 2019 (COVID-19) from X-ray images,” Medical Hypotheses, vol. 140, Article ID 109761, 2020.
35. A. I. Khan, J. L. Shah, and M. M. Bhat, “CoroNet: a deep neural network for detection and diagnosis of COVID-19 from chest x-ray images,” Computer Methods and Programs in Biomedicine, vol. 196, Article ID 105581, 2020.
36. Hussain, L., Nguyen, T., Li, H., Abbasi, A. A., Lone, K. J., Zhao, Z., ... & Duong, T. Q. (2020). Machine-learning classification of texture features of portable chest X-ray accurately classifies COVID-19 lung infection. BioMedical Engineering OnLine, 19(1), 1-18.
37. Zargari Khuzani, A., Heidari, M., & Shariati, S. A. (2021). COVID-Classifier: An automated machine learning model to assist in the diagnosis of COVID-19 infection in chest x-ray images. Scientific Reports, 11(1), 1-6.
38. Ghosh, Madhumala, Devkumar Das, and Chandan Chakraborty. “Entropy based divergence for leukocyte image segmentation.” 2010 International Conference on Systems in Medicine and Biology. IEEE, 2010, pp:409-413.
39. Tek, F. Boray, Andrew G. Dempster, and Izzet Kale. “Parasite detection and identification for automated thin blood film malaria diagnosis.” Computer vision and image understanding 114.1 (2010): 21-32.
40. Galloway, M. M. “Texture classification using gray level run length.” Computer graphics and image processing 4.2 (1975): 172-179.
41. Krishnan, M. Muthu Rama, et al. “Statistical analysis of textural features for improved classification of oral histopathological images.” Journal of medical systems 36.2 (2012): 865-881.
42. Sarkar, Nirupam, and Bidyut Baran Chaudhuri. “An efficient differential box-counting approach to compute fractal dimension of image.” IEEE Transactions on systems, man, and cybernetics 24.1 (1994): 115-120.
43. Krishnan, M. Muthu Rama, et al. “Textural characterization of histopathological images for oral sub-mucous fibrosis detection.” Tissue and Cell 43.5 (2011): 318-330.
44. Gonzalez, R. C. Processing, (2002).

45. Das, Devkumar, et al. “Invariant moment based feature analysis for abnormal erythrocyte recognition.” 2010 International Conference on Systems in Medicine and Biology. IEEE, 2010, pp: 242-247.
46. Rey, Denise, and Markus Neuhäuser. “Wilcoxon-signed-rank test.” International encyclopedia of statistical science.Springer Berlin Heidelberg, 2011. 1658-1659.
47. Ghasemi, Asghar, and Saleh Zahediasl. “Normality tests for statistical analysis: a guide for non-statisticians.” International journal of endocrinology and metabolism 10.2 (2012): 486.
48. McKnight, Patrick E., and Julius Najab. “Mann Whitney U Test.” The Corsini encyclopedia of psychology (2010): 1-1.
49. Budak, H. and Tas ¸abat, S.E. “A modified t-score for feature selection”, Anadolu U niversitesi € Bilim Ve Teknoloji Dergisi A-Uygulamalı Bilimlerve Muhendislik € , 2016, Vol. 17 No. 5, pp. 845-852.
50. t-table. http://www.sjsu.edu/faculty/gerstman/StatPrimer/t-table.pdf. 2017.
51. M. Shasidhar , V.Sudheer Raja, B. Vijay Kumar, “MRI Brain Image Segmentation Using Modified Fuzzy C-Means Clustering Algorithm”,IEEE International Conference on Communication Systems and Network Technologies, 2011.
52. Dr. S. Vasundra et.al, “A Fuzzy C-Means Based Feature Selection to Process Medical Data”, International Journal on Recent and Inno0vation Trends in Computer and Communication, ISSN: 2321-8169, July 2017. IJRITCC
53. Matsuki, Kazunaga, Victor Kuperman, and Julie A. Van Dyke. “The Random Forests statistical technique: An examination of its value for the study of reading.” Scientific Studies of Reading 20.1 (2016): 20-33.
54. Airola, Antti, et al. “An experimental comparison of cross-validation techniques for estimating the area under the ROC curve.” Computational Statistics & Data Analysis 55.4 (2011): 1828-1844.